Effect of magnetic dipolar interactions on nanoparticle heating efficiency: Implications for cancer hyperthermia

Luis C. Branquinho[1], Marcus S. Carrião[1], Anderson S. Costa[1], Nicholas Zufelato[1], Marcelo H. Sousa[2], Ronei Miotto[3], Robert Ivkov[4] and Andris F. Bakuzis[1,*]

[1] Instituto de Física, Universidade Federal de Goiás, 74001-970, Goiânia-GO, Brazil,
[2] Faculdade de Ceilândia, Universidade de Brasília, 72220-140, Brasília-DF, Brazil,
[3] Centro de Ciências Naturais e Humanas, Universidade Federal do ABC, Rua Santa Adélia, 166, CEP 09210-170, Santo André, SP, Brazil,
[4] Department of Radiation Oncology and Molecular Radiation Sciences, Johns Hopkins University School of Medicine, Baltimore, MD 21287, USA.

Supplementary material

Supplementary material

S1 – **Linear response regime**

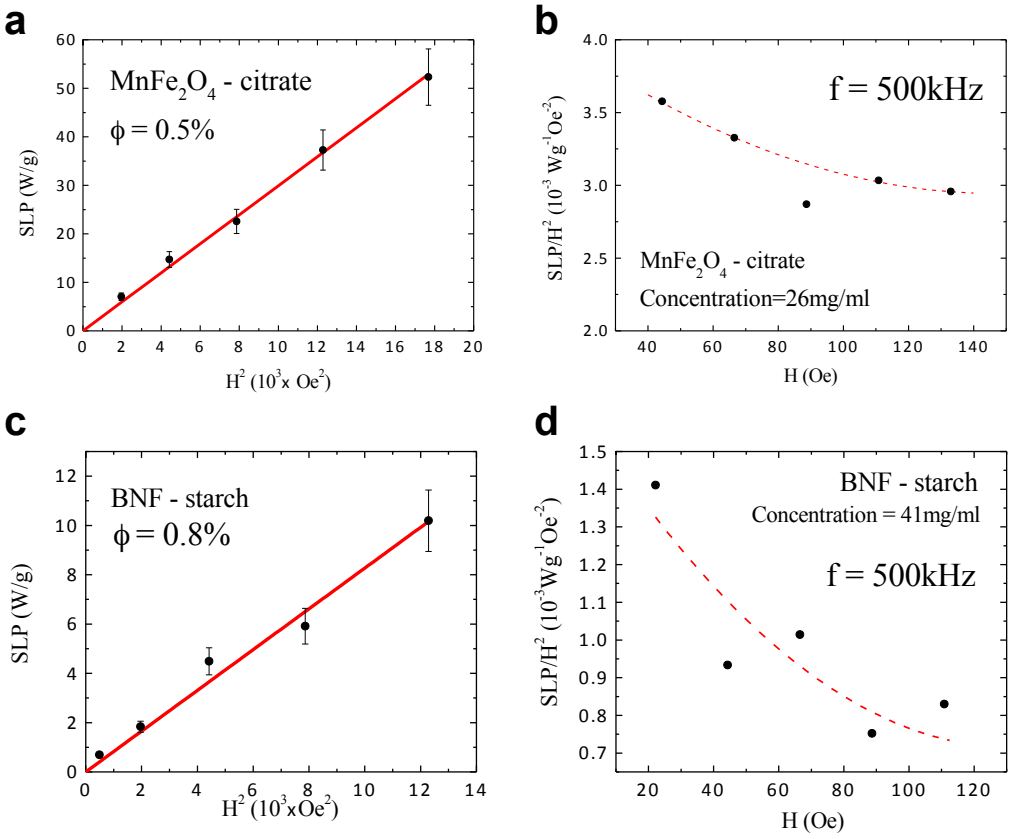

Figure S1. (a) Specific loss power (SLP) as function of the square of the magnetic field for the MNF-citrate sample at a particle volume fraction of 0.51%. Symbols represent experimental data while the solid line corresponds to a linear fit of the data. (b) Efficiency (defined as SLP/H^2) as function of the magnetic field at the same particle concentration (26mg/mL). Decreasing SLP with increasing magnetic field indicates that the sample is at the low barrier regime (see theoretical discussion on Ref. 7). (c) Specific loss power (SLP) as function of the square of the magnetic field for the BNF-starch sample at a particle volume fraction of 0.8%. Symbols represent experimental data while the solid line corresponds to a linear fit of the data. (d) SLP/H^2 as function of the magnetic field for the same particle concentration (41mg/mL).

S2 – **Theoretical calculations for fanning and coherent dimers**

Coherent rotation

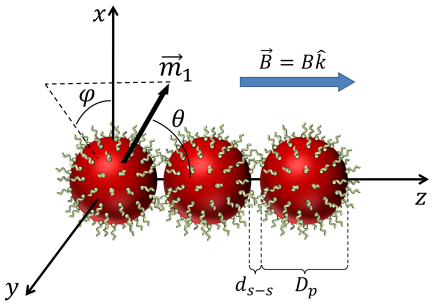

The dipolar interaction term in SI units for a coherent dimer is given by

$$E_{dip}^{co} = -\frac{\mu_0}{4\pi}\frac{\vec{m}_1}{r^3}\cdot[3(\vec{m}_2\cdot\hat{r})\hat{r} - \vec{m}_2] = -\frac{\mu_0}{4\pi}\frac{1}{r^3}[3m^2cos^2(\theta) - m^2]$$

$$E_{dip}^{co} = \frac{\mu_0}{4\pi}\frac{m^2}{r^3}3\sin^2(\theta) - \frac{\mu_0}{4\pi}\frac{2m^2}{r^3}$$

Dividing by $2V_p$, the dipolar contribution term to the free energy density is given by

$$F_{dip}^{co} = \frac{\mu_0}{4\pi}\frac{3V_pM_S^2}{2r^3}\sin^2(\theta) - \frac{\mu_0}{4\pi}\frac{V_pM_S^2}{r^3}$$

Fanning rotation

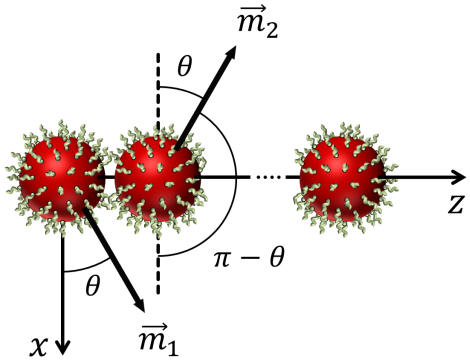

The dipolar interaction term in SI units for a fanning dimer is given by

$$E_{dip}^{fan} = -\frac{\mu_0}{4\pi}\frac{\vec{m}_1}{r^3}\cdot[3(\vec{m}_2\cdot\hat{r})\hat{r} - \vec{m}_2] = -\frac{\mu_0}{4\pi}\frac{1}{r^3}[3m^2cos^2(\theta) - m^2\cos(2\theta)]$$

$$E_{dip}^{fan} = \frac{\mu_0}{4\pi}\frac{m^2}{r^3}\sin^2(\theta) - \frac{\mu_0}{4\pi}\frac{2m^2}{r^3}$$

Dividing by $2V_p$, the dipolar contribution term to the free energy density is given by

$$F_{dip}^{fan} = \frac{\mu_0}{4\pi}\frac{V_p M_S^2}{2r^3}\sin^2(\theta) - \frac{\mu_0}{4\pi}\frac{V_p M_S^2}{r^3}$$

Note that the dipolar contribution has a similar effect as the anisotropy term ($K\sin^2(\theta)$), i.e. both terms have a sine square dependence in the free energy. Nevertheless, the dipolar contribution term to the effective anisotropy of both dimers, coherent and fanning, differs by a factor of 3.

In CGS units, the dipolar contribution to the free energy density for both dimers is written as

$$F_{dip}^{co} = \frac{3V_p M_S^2}{2r^3}\text{sen}^2(\theta) - \frac{V_p M_S^2}{r^3}$$

$$F_{dip}^{fan} = \frac{V_p M_S^2}{2r^3}\text{sen}^2(\theta) - \frac{V_p M_S^2}{r^3}$$

The differences between the fanning and coherent dimers to the SLP calculations can be found below. We can now show similar calculations as Fig. 4 in the manuscript, but now specifically for the different dimers.

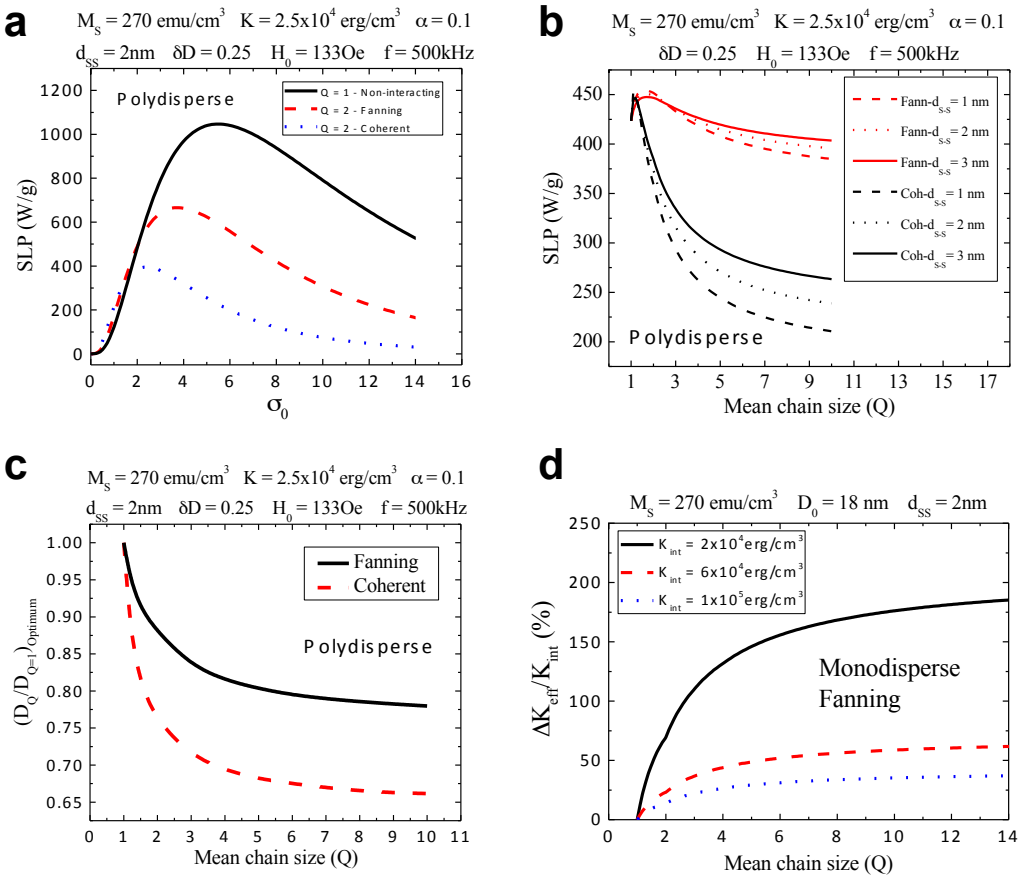

Figure S2. (a) SLP as function of dimensionless anisotropy term for a poly-disperse sample considering the non-interacting case (Q=1) and the different dimers (Q=2), i.e. coherent and fanning and field amplitude of 133Oe. (b) SLP as function of chain size for the different dimers considering a poly-disperse system and distinct surface-to-surface distances. (c) Optimum hyperthermia size ratio as function of chain size for the distinct dimers and a surface-to-surface distance of 2nm. (d) Monodisperse calculation of the relative anisotropy increase $\frac{\Delta K}{K(Q=1)} = \frac{K(Q)-K(Q=1)}{K(Q=1)}$ as function of mean chain size for distinct intrinsic magnetic anisotropy values (fanning configuration). Note that the effect increases lowering the nanoparticle (intrinsic, i.e. non-interacting) magnetic anisotropy value.

S3 – **Electron magnetic resonance (EMR) data**

Note that different from NMR, where the magnetic field is constant, and one changes the frequency of the electromagnetic field (note that we are not discussing NMRI), in EMR, the frequency is fixed, i.e. the (low amplitude) ac electromagnetic field frequency is constant (in our case around 9.4Ghz, x-band – microwave), and is applied perpendicular to the DC field. Also, the DC applied magnetic field is changed in order to achieve the resonance field condition. The resonance condition is detected through a microwave absorption at a given field range. Indeed, the electron magnetic resonance occurs when the energy difference between two states (which is changed by sweeping the magnetic field, and dependent upon the effective field felt by the electron spins) is equal to the microwave electromagnetic energy. So, note that in EMR one does not have a fixed 0.3T applied to the sample. Actually the field sweeps from 5mT up to 0.5T. Maximum absorption (resonance) is occurring at around 0.3T for the samples investigated in this work.

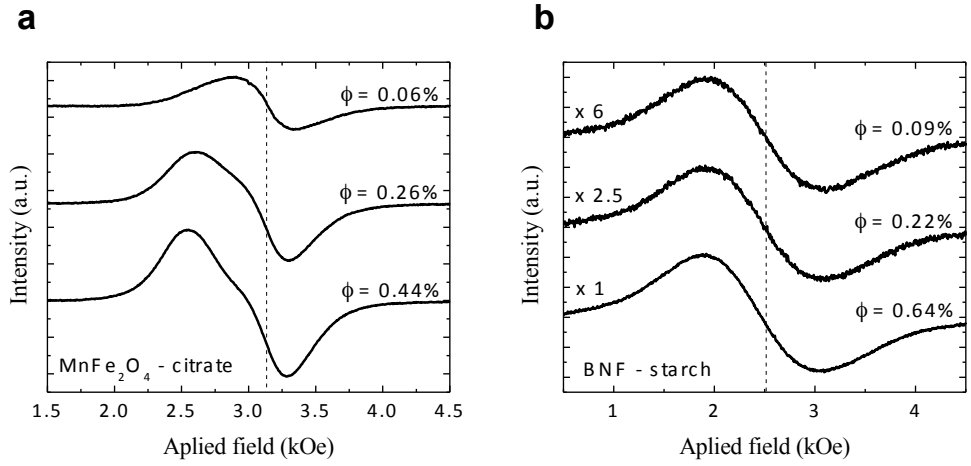

Figure S3. (a) X-band electron magnetic resonance spectra of different particle volume fractions of the MNF colloid. (b) EMR of some representative particle concentrations of the BNF sample.

S4 – **Magnetic birefringence data**

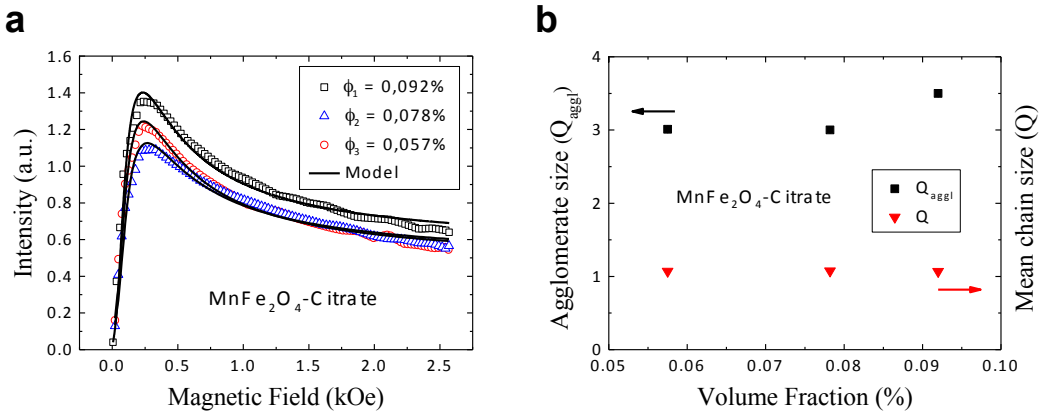

Figure S4. (a) Static magnetic birefringence (SMB) intensity as function of the magnetic field for different particle volume fraction MNF-citrate samples. Symbols represent experimental data while the solid line corresponds to the best fit of the data using a theoretical model based upon Ref. S1 and 36. The model contained just two parameters that were related to the chain size and the surface-to-surface distance between nanoparticles forming the linear chain. (b) Mean chain size (agglomerate size) as function of the particle volume fraction. The model enable us to estimate the agglomerate size as well as the percentage of particles forming chains (since isolated spherical nanoparticles do not contribute to the SMB data). From this we obtained the mean chain size (Q≈1.1), which was found to be close (but lower) to the electron magnetic resonance analysis (see Fig. 2(d) – Q between 1.1-1.3) at this particle concentration range. (Details on the experimental set up can be found in Ref. 37).

[S1] Xu, M. & Ridler, P. J. Linear dichroism and birefringence effects in magnetic fluids. *J. Appl. Phys.* **82**, 326-332 (1997).

S5 – **Three dimensional polydisperse Monte Carlo simulations**

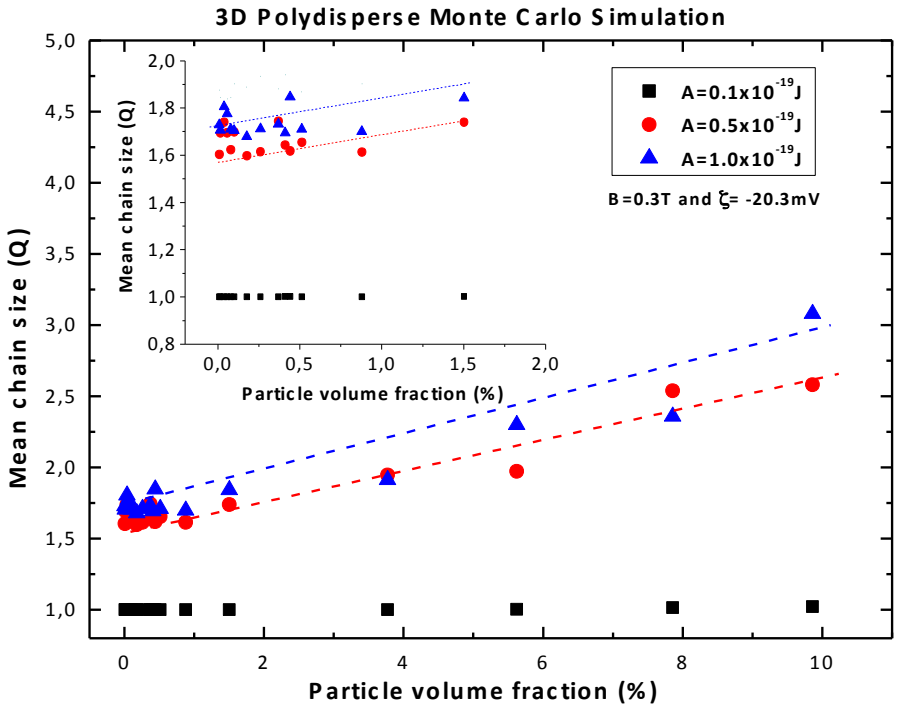

Figure S5. Three-dimensional polydisperse Monte Carlo simulations for the MNF-citrate sample (see Ref. 14 for details on the algorithm). Nanoparticles are considered spherical. The simulation used a zeta potential of -20.3mV (that corresponds to a number of molecules of 1.2×10^{17}mol/m^2 – see Ref. 14), an external magnetic field of 0.30 T (close to the EMR field) and three distinct Hamaker constants, namely A=0.1, 0.5 and 1.0 x 10^{-19} J. The size distributions follows the experimental TEM parameters (see Fig. 2 (b)). The simulation indicates that small agglomerates can be found even at the low particle concentration range depending upon the Hamaker and zeta potential (which is related to the grafting, i.e. the number of molecules at the nanoparticle surface) parameters. The quantitative differences between the experimental data (see Fig. 2(d)) and MC simulation is expected due to possible desorption of coating molecules and depletion effect (The MC simulation does not take into account ion-ion correlations in the electrostatic interaction – see Ref. 14). Nevertheless one can clearly observe the same trend as the EMR analysis, i.e. chain lenght increases with increasing concentration. The inset shows the same MC data at a lower concentration range. As expected, chain length increases with increasing Hamaker constant and particle concentration. Dashed lines are guide to the eye.

S6 – **Chain size theoretical model: High field and zero field limit**

According to the literature,[14,38] the dependence of the mean chain size on the volume fraction is given by $< Q >= 2\varphi e^{E}/\left(\sqrt{1+4\varphi e^{E}}-1\right)$, with φ the particle volume fraction and E a dimensionless energy parameter between particles in the chain. In the flexible chain model, this parameter for zero field condition, reads $E_{H=0} = 2\lambda - \ln(3\lambda^3)$, whereas at the high field limit $E_{H\to\infty} = 2\lambda - \ln(3\lambda^2)$. [38,S2]

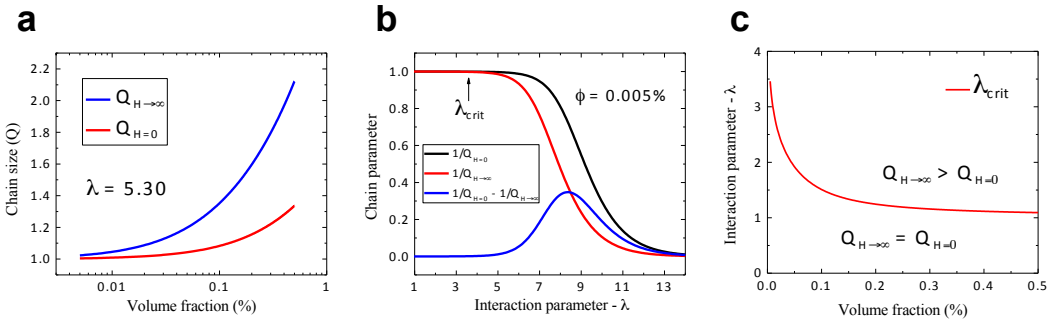

Figure S6. (a) Chain size as function of particle volume fraction for the high and zero field cases for a constant interaction parameter value, i.e. λ=5.3. (b) The inverse of chain size (1/Q) as function of the interaction parameter for the two limiting cases, H=0 (black line) and $H \to \infty$ (red line) at a fixed volume fraction, phi=0.005%. The blue line is the difference between the inverse of the zero field chain size to the high field one. Note that the model indicates that only above a "critical" interaction parameter λ_{crit}, one observes significant differences between both estimations. (c) A phase-like diagram indicating how the λ_{crit} depends upon the volume fraction. This estimation assumed a difference value of 0.5% between the chain sizes. If $\lambda < \lambda_{crit}$ both chain sizes can be assumed to have the same value, while for $\lambda > \lambda_{crit}$ the chain size at both limits are very distinct. From EMR experimental data we estimate for the MNF sample λ=5.3.

[S2] Zubarev, A. Yu., Iskakova, L. Yu. Theory of structural transformations in ferrofluids: Chains and "gas-liquid" phase transitions. Phys. Rev E 65, 061406 (2002).

S7 – Characteristic time (τ_0) and damping influence on SLP

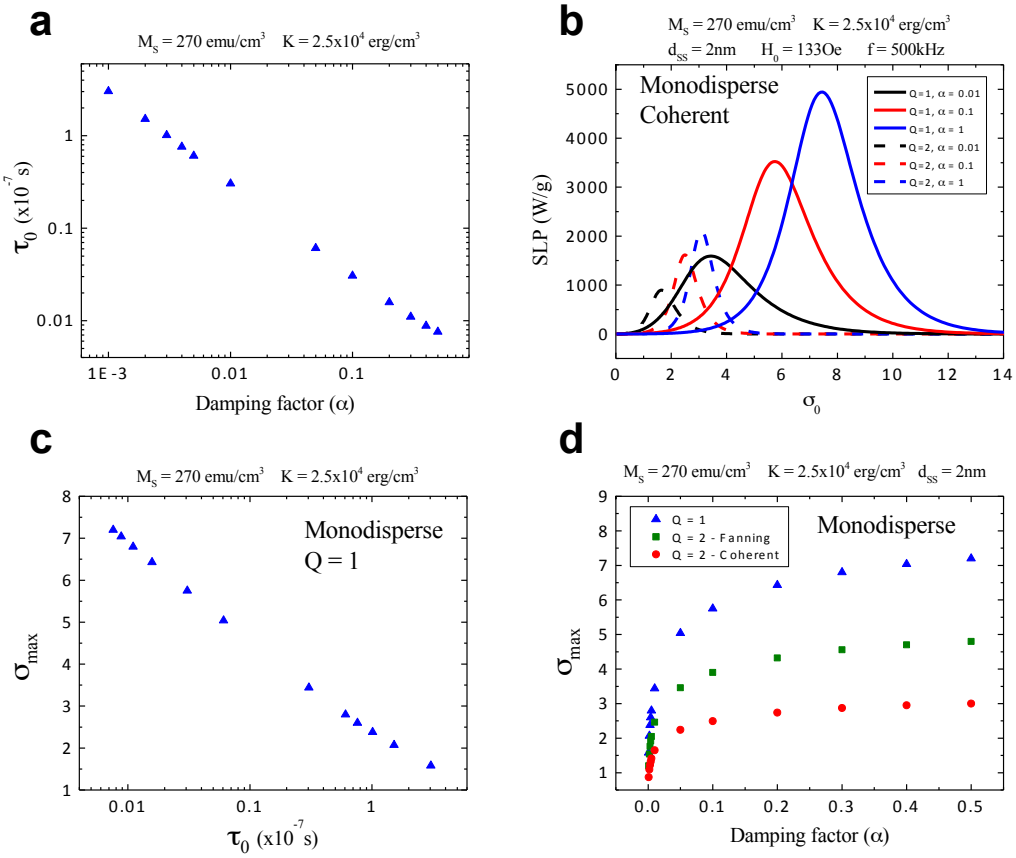

Figure S7. (a) In this figure is shown how the characteristic time τ_0 changes for distinct damping factor values**.** Note that increasing the damping value results in a decrease of τ_0. **(b)** SLP as function of the anisotropy dimensionless parameter for different damping values (τ_0). The non-interacting case (Q=1) and the dimer (Q=2) is shown. A SLP maximum is observed indicating the existence of optimum anisotropy values. Increasing the characteristic time (or decreasing the damping value) shifts the maximum anisotropy to lower values, and decreases the maximum SLP. (c) Optimum anisotropy values as function of τ_0. **(d)** Optimum anisotropy values as function of the damping fator for the non-interacting case (Q=1), and dimers (Q=2) in the fanning and coherent configuration. Note that for high damping values the optimum anisotropy changes only slightly. This observation is consistent with recent dynamic hysteresis simulations.[25] The chain formation reduces both SLP and optimum anisotropy values.

S8 – High field amplitude SLP concentration dependence

For the high field amplitude study of the SLP concentration dependence we used a different hyperthermia system. The magnetic hyperthermia equipment consisted of an Ambrell system model EasyHeat-LI. The system operated at 300kHz with an 8-turn coil, which was cooled using a closed-loop circulating water system. The temperature was measured using a fiber-optic system. Again, the amplitude of the alternating magnetic fields was obtained from measurements using an ac field probe bought from AMF Lifesystems.

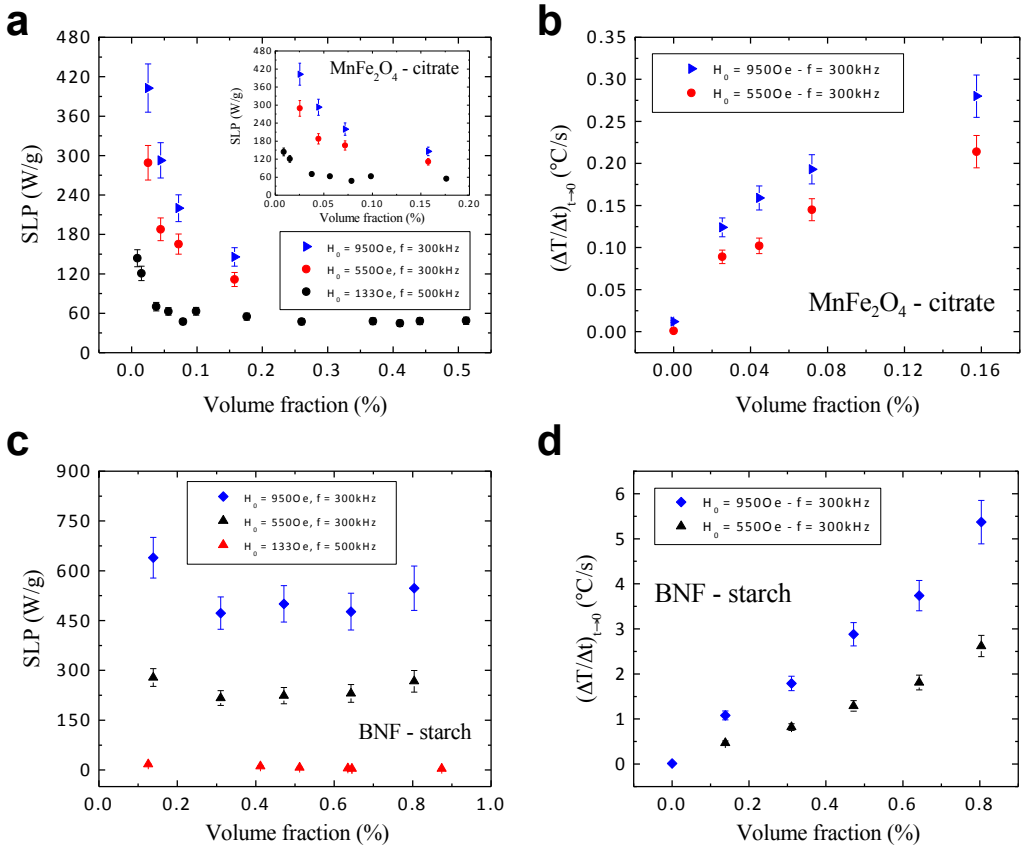

Figure S8. (a) SLP as function of particle volume fraction. Black circles correspond to the MNF-citrate data at a frequency (f) of 500kHz and 133Oe. The other measurements were performed at f=300kHz. Red circles correspond to data at 550Oe, while triangles the field amplitude is 950Oe. Note that one can undoubtedly observe a decrease of SLP the larger the particle concentration (chain size). In those high field measurements the chain size can be calculated assuming the EMR data, with λ=5.3 and using each particle volume fraction value (determined from VSM measurements). The inset shows the same data at a lower concentration range. (b) Initial heating rates of the MNF-citrate samples for data at 300kHz. The 500kHz data appears in the inset of Fig. 1(d) of the paper. (c) SLP as function of particle volume fraction for the BNF-starch sample. (d) Initial heating rates as function of concentration of the BNF samples for data at 300 kHz.

S9 – High field amplitude SLP chain size dependence

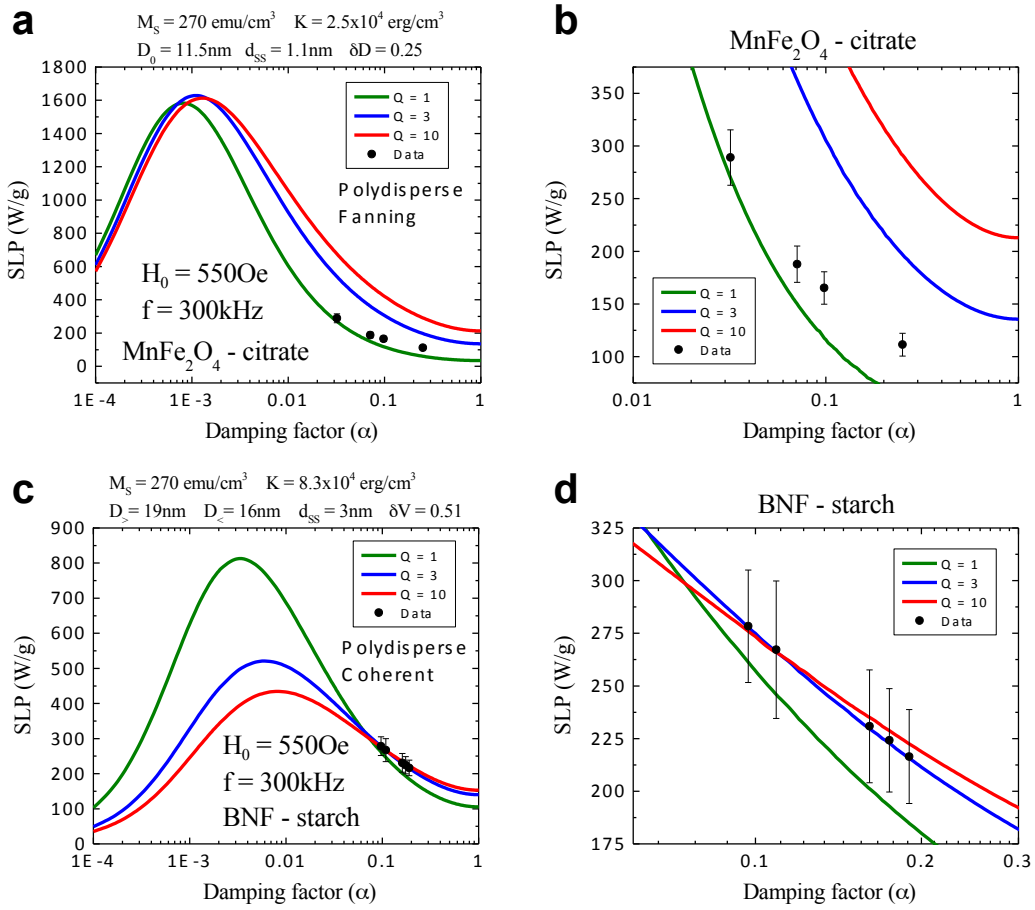

Figure S9. (a) SLP as function of damping factor for the cases Q=1, 3 and 10. Polydisperse theoretical calculations used the experimental parameters of the samples. Symbols represent the experimental data of the MNF-citrate sample. The error bars can not be observed at this scale. (b) SLP as function of damping factor at a smaller damping range for the MNF-citrate sample. (c) SLP as function of damping factor for the cases Q=1, 3, 10. Symbols represent the experimental data of the BNF-starch sample. (d) SLP as function of damping factor at a smaller damping range for the BNF-starch sample. Theoretical calculations of the parallelepiped-shaped nanoparticles considered the volume distribution. Note that for both samples we found an increase in the chain size increasing the particle volume fraction. For the MNF-citrate, at the high field limit, the chain length changes from 1 to 2.5. While the BNF sample this range is within 2.5 to 3.5. At this range, and due to the experimental error bars, it is now clear why the BNF sample had not shown any significant SLP concentration dependence. On the contrary, the MNF-citrate shows a strong SLP concentration (chain size) dependence at this experimental condition.